- 1 Methane dynamics regulated by microbial community response to permafrost thaw
- 3 Carmody K. McCalley<sup>1†</sup>‡, Ben J. Woodcroft<sup>2</sup>, Suzanne B. Hodgkins<sup>3</sup>, Richard A. Wehr<sup>1</sup>, Eun-
- 4 Hae Kim<sup>4</sup>, Rhiannon Mondav<sup>2†</sup>, Patrick M. Crill<sup>5</sup>, Jeffrey P. Chanton<sup>3</sup>, Virginia I. Rich<sup>4</sup>, Gene
- 5 W. Tyson<sup>2</sup>, and Scott R. Saleska<sup>1</sup>‡
- 7 Department of Ecology and Evolutionary Biology, University of Arizona, Tucson, AZ, 85721,
- 8 USA

2

6

- 9 <sup>2</sup>Australian Centre for Ecogenomics, School of Chemistry and Molecular Biosciences,
- 10 University of Queensland, Brisbane, 4072, Australia.
- <sup>3</sup>Department of Earth, Ocean and Atmospheric Science, Florida State University, Tallahassee,
- 12 FL, 32306, USA
- <sup>4</sup>Department of Soil, Water and Environmental Science, University of Arizona, Tucson, AZ,
- 14 85721, USA
- <sup>5</sup>Department of Geological Sciences, Stockholm University, Stockholm 106 91, Sweden
- <sup>†</sup>Present address: Earth Systems Research Center, University of New Hampshire, Durham, NH,
- 17 03824, USA (C.K.M). Department of Ecology and Genetics, Uppsala University, Uppsala 75
- 18 236, Sweden (R.M)

21

- <sup>‡</sup>Corresponding authors. Email: carmody.mccalley@unh.edu (C.K.M),
- 20 saleska@email.arizona.edu (S.R.S)
- Permafrost contains approximately 50% of global soil carbon<sup>1</sup>. It is thought that
  permafrost thaw can lead to soil carbon loss in the form of methane and carbon dioxide
  emissions<sup>2,3</sup>. The magnitude of the resulting positive climate feedback of such greenhouse

gas emissions remains uncertain<sup>3</sup> and may to a large extent depend on the poorly understood role of microbial community composition in regulating the metabolic processes that drive such ecosystem-scale greenhouse gas fluxes. Here we use a natural landscape gradient of permafrost thaw in northern Sweden<sup>4,5</sup>, as a model to investigate the role of microbial communities in regulating methane cycling, and to test whether knowledge of community dynamics could improve predictions of carbon emissions under permafrost loss. We find that changing vegetation and increasing methane emissions with permafrost thaw are associated with a switch from hydrogenotrophic to partially acetoclastic methanogenesis, resulting in a large shift in the  $\delta^{13}$ C signature (10-15‰) of emitted methane. Abundance of the methanogen, Candidatus Methanoflorens stordalenmirensis<sup>6</sup>, is a key predictor of the methane isotope shifts, which in turn predicts the proportion of carbon emitted as methane versus carbon dioxide, an important factor for simulating the climate feedback associated with permafrost thaw in global models<sup>3,7</sup>. By showing that the abundance of key microbial lineages can be used to predict atmospherically relevant patterns in methane isotopes and the proportion of carbon metabolized to methane during permafrost thaw, we establish a basis for scaling changing microbial communities to ecosystem isotope dynamics. Our findings suggest that microbial ecology can play an important role in the ecosystem scale responses to global change.

25

26

27

28

29

30

31

32

33

34

35

36

37

38

39

40

41

42

43

44

45

46

Multiple factors—including hydrology, vegetation, organic matter chemistry, pH, and soil microclimate—are affected by permafrost loss<sup>5,8,9</sup>. Together these factors regulate microbial metabolisms that release carbon dioxide (CO<sub>2</sub>) and methane (CH<sub>4</sub>) from thawing permafrost<sup>10–12</sup>, and are the basis for earth system model predictions of future CH<sub>4</sub> emissions<sup>7,13,14</sup>. However, the

role of microbial community composition in regulating the metabolic processes that drive ecosystem-scale fluxes is unknown.

At our study site in Stordalen, as in other thawing permafrost peatlands<sup>8,15</sup>, permafrost loss causes hydrologic and vegetation shifts: well-drained permafrost-supported palsas collapse into partially-thawed moss-dominated (*Sphagnum* spp.) bogs and fully-thawed sedge-dominated (e.g. *Eriophorum angustifolium*) fens<sup>4</sup>. Between 1970 and 2000, 10% of Stordalen's palsa habitat thawed into such wetlands<sup>4</sup>. This transition drives an appreciable global warming impact because CO<sub>2</sub>-emitting palsa is converted to bogs and fens which take up CO<sub>2</sub> but emit CH<sub>4</sub> (a more potent greenhouse gas<sup>3</sup>)<sup>4,5,16</sup>. The net effect is that the high methane-emitting fen contributes 7 times the greenhouse impact per unit area as the palsa. This thaw progression is also associated with an increase in overall organic matter lability, including a decrease in C:N and an increase in humification rates<sup>9</sup>. We hypothesized, consistent with previous studies of *in situ* bog and fen systems<sup>17–19</sup>, that thaw progression also facilitates a shift from hydrogenotrophic to acetoclastic CH<sub>4</sub> production.

We used the distinct isotopic signatures of different microbial CH<sub>4</sub> production and consumption pathways to directly relate changes in CH<sub>4</sub> dynamics across the thaw gradient to underlying changes in the microbial community. Methane produced by hydrogenotrophic methanogens generally has lower  $\delta^{13}$ C and higher  $\delta D$  ( $\delta^{13}$ C = -110 to -60% and  $\delta D$  = -250 to -170%) relative to that produced by acetoclastic methanogens ( $\delta^{13}$ C = -60 to -50% and  $\delta D$  = -400 to -250%)<sup>19,20</sup>. If methanotrophic microbes then oxidize CH<sub>4</sub>, lighter molecules are preferentially consumed, leaving the remaining CH<sub>4</sub> <sup>13</sup>C- and D-enriched relative to the original CH<sub>4</sub> pool (see expected patterns in Extended Data Fig 1)<sup>19,20</sup>.

High temporal-resolution measurements of the magnitude and isotopic composition of CH<sub>4</sub> emissions, using a quantum cascade laser spectrometer (QCLS, Aerodyne Research Inc.) connected to autochambers, showed that CH<sub>4</sub> emissions and their <sup>13</sup>C content increased with thaw. Average CH<sub>4</sub> fluxes increased from effectively zero at the intact permafrost palsa site to  $1.46 (\pm 0.37) \text{ mg CH}_4 \text{ m}^{-2} \text{ h}^{-1}$  at the thawing *Sphagnum* site, to 8.75 ( $\pm 0.50$ ) mg CH<sub>4</sub> m<sup>-2</sup> h<sup>-1</sup> at the fully thawed *Eriophorum* site (Fig. 1a, p < 0.001). The average  $\delta^{13}$ C of emitted CH<sub>4</sub> also increased significantly, from -79.6% ( $\pm 0.9$ ) in the *Sphagnum* site to -66.3% ( $\pm 1.6$ ) in the *Eriophorum* site (Fig. 1b, p= 0.03). This consistent 10-15‰ divergence between sites was maintained through the growing season but overlain by parallel fluctuations in  $\delta^{13}$ C-CH<sub>4</sub>. suggesting that weather patterns exerted a common influence over the magnitude of isotopic fractionation. Porewater CH<sub>4</sub> isotopes showed a similar pattern, with *Eriophorum* site porewater  $\delta^{13}$ C ~10% higher than *Sphagnum* (July and August, Fig. 1b, Extended Data Table 1). Porewater CH<sub>4</sub> was <sup>13</sup>C-enriched by 5-20% relative to emitted CH<sub>4</sub>, as expected due to diffusive fractionation (Methods equation (2)) <sup>18,21</sup>.

The apparent fractionation factor for carbon in porewater  $CH_4$  relative to  $CO_2$ ,  $\alpha_C$  (Methods equation (2), Extended Data Table 1), is a related index of changes in  $CH_4$  production<sup>22</sup>. Greater fractionation is associated with hydrogenotrophic methanogenesis, and was found in the thawing Sphagnum site (average  $\alpha_C = 1.053 \pm 0.002$ ). Significantly less fractionation (p=0.002) associated with more acetoclastic production or with consumption by oxidation was found in the fully thawed Eriophorum porewater (average  $\alpha_C = 1.046 \pm 0.001$ ). Here, increases in acetoclastic production, not oxidation, best explain isotopic shifts because lower  $\alpha_C$  and higher  $\delta^{13}C$ - $CH_4$  are accompanied by significantly lower  $\delta D$ - $CH_4$  (Extended Data Fig. 1, p< 0.001)<sup>19</sup>. This is consistent with the pattern of isotopes in  $CH_4$  emissions as well as

incubations of Stordalen peat<sup>9</sup> and studies showing bog-to-fen shifts from hydrogenotrophic to acetoclastic methanogenesis<sup>17–19</sup>.

The CH<sub>4</sub> flux and isotope results provide compelling but indirect evidence for changes in CH<sub>4</sub>-cycling microbial communities with permafrost thaw. These microbiological changes could be shifts in activity of particular community members or changes in community composition. We examined the role of community composition through 16S rRNA gene amplicon sequencing. All known methanogens belong to a small number of archaeal lineages within the Euryarchaeota<sup>23</sup>. As expected, the shift from CH<sub>4</sub>-neutral intact permafrost palsa to CH<sub>4</sub>-emitting wetland corresponded to a substantial increase in the relative abundance of methanogenic archaeal lineages (Fig. 1c, Extended Data Table 2,3). In the aerobic palsa and surface *Sphagnum* habitats, methanogens were found in low relative abundance (average <0.6%), while the anaerobic environments of the *Eriophorum* and deeper (below the water table) *Sphagnum* habitats harbored communities with a substantially higher relative abundance of methanogens (20-30%).

More significantly, the abundance of specific methanogenic lineages varied across the thaw gradient (Fig. 1c, Extended Data Table 2) in a manner corresponding to shifts in CH<sub>4</sub> production mechanism inferred from the isotope data (Fig. 1b). At the partially thawed *Sphagnum* site, where CH<sub>4</sub> isotopes were more hydrogenotrophic, the methanogen community was dominated by hydrogenotrophic populations (>=57% of sequences). Members of the genus *Methanobacterium* and close relatives of the recently described hydrogenotroph, Candidatus '*Methanoflorens stordalenmirensis*'<sup>6</sup> (a partial genome of which has also been identified in incubations of Alaksan permafrost<sup>12</sup>), were the most abundant phylotypes. While present, the metabolically versatile *Methanosarcina* (capable of utilizing a wide range of substrates including acetate and hydrogen<sup>24</sup>), was much less abundant, averaging ~15% of the methanogen sequences.

At the fully thawed *Eriophorum* site (where isotope signatures shifted towards acetoclastic), members of the obligately acetoclastic genus *Methanosaeta* increased in abundance, comprising approximately one-third of the methanogenic population. The remaining methanogenic community was taxonomically diverse, including lineages present at the *Sphagnum* site as well as an additional hydrogenotrophic genus, *Methanoregula* (Extended Data Table 2). Differences in the functional (hydrogenotrophic versus acetoclastic) composition of the methanogen community between the sites were smallest in October, coinciding with a convergence in  $\delta^{13}$ C-CH<sub>4</sub> (Fig. 1a and Extended Data Table 2,3).

Together, the isotope and microbial sequence data suggest that microbial community shifts drive large, concordant variations in CH<sub>4</sub> isotope biogeochemistry both seasonally and during permafrost thaw, a novel observation at the ecosystem scale. The early successional hydrogenotroph '*M. stordalenmirensis*' dominates methanogenic metabolism in the early stages of thaw, followed by the subsequent emergence of a more diverse methanogen community, including obligate acetoclastic methanogens. This microbial succession provides direct evidence for how changes in ecosystem structure during permafrost thaw (plant succession and increases in organic matter quality<sup>9</sup>) translate into altered CH<sub>4</sub> biogeochemistry.

To quantify the effect of this shifting microbial community composition for  $CH_4$  isotopic patterns, we examined the relationships between isotope fractionation ( $\alpha_C$ ), environmental conditions known or expected to impact methanogenesis, and the relative abundance of specific methanogenic lineages (Extended Data Table 4). Surprisingly, rather than a functional group (such as hydrogenotrophic methanogens), a single organism -- the hydrogenotroph 'M. stordalenmirensis' -- was the best one-variable predictor of isotopic patterns in the field (Fig. 2a). Several variables that typically differentiate bogs and fens, including pH and water table

depth<sup>18</sup>, were significant predictors of  $\alpha_C$ , however, it was the relative abundance of 'M. stordalenmirensis' that explained both the large range of  $\alpha_C$  observed at the Sphagnum site ( $R^2 = 0.7$ , p < 0.001) as well as patterns across sites ( $R^2 = 0.6$ , p < 0.001). This suggests, contrary to the current practice of focusing on community functional diversity, that an individual microbial lineage can have a disproportionate influence on ecosystem biogeochemistry.

Stepwise regression identified environmental variables (water table depth, peat C:N and peat  $\delta^{13}$ C) that improved model predictions of  $\alpha_{\rm C}$  (to  $R^2$  = 0.8, p<0.001). While confirming the central importance of '*M. stordalenmirensis*' in explaining variation in  $\alpha_{\rm C}$  (Extended Data Table 5) this model also supports the hypothesis that organic matter chemistry underlies shifts in CH<sub>4</sub> metabolism<sup>9,25</sup>. Interestingly, the dependence on the abundance of this lineage was evident despite the relative rather than absolute nature of the community composition analysis, and measurement of abundance rather than activity. We hypothesize that direct measures of gene expression or metabolic activity (meta-transcriptomics and –proteomics) will have an even stronger association than community composition data with isotopic signatures.

Further analysis showed that  $\alpha_C$  significantly correlates ( $R^2$  = 0.7, p=0.004) with the large range in CH<sub>4</sub>:CO<sub>2</sub> production ratio (0.13-0.84) measured in anaerobic incubations of Stordalen peat (Fig. 2b). Thus it is likely that changes in the proportion of anaerobically mineralized C that ends up as CH<sub>4</sub>—a key, but poorly constrained parameter in global CH<sub>4</sub> models<sup>26</sup>—tracks the abundance of 'M. stordalenmirensis , which acts as an index of the concerted changes in microbial community and organic matter chemistry that together control the efficiency of carbon metabolism.

Incorporating this understanding of the imprint of microbial communities could be critical to (1) improved model prediction of future climate change CH<sub>4</sub> feedbacks and (2)

accurate attribution of the portion of global atmospheric CH<sub>4</sub> change that derives from permafrost thaw. First, in simulating CH<sub>4</sub> cycling, earth system models typically prescribe as fixed the fraction of anaerobically metabolized carbon that becomes CH<sub>4</sub><sup>26</sup>. The lack of a basis for predicting this parameter across ecosystems and in response to climate change limits current modeling efforts (3). Our finding that the CH<sub>4</sub>:CO<sub>2</sub> production ratio is highly variable and predictable from isotopic indicators of methanogenic community composition (Fig. 2b) supports improving representation of microbial ecology in models<sup>17,27</sup>. While simulating microbial population dynamics is beyond the scope of current global models, identification of microbial lineages that predict key parameters, such as the CH<sub>4</sub>:CO<sub>2</sub> ratio, provides insights that improve simulations of CH<sub>4</sub> biogeochemistry used to estimate global emissions.

Second, atmospheric inversion studies which use CH<sub>4</sub> mixing ratios and isotopes to infer global sources and sinks of atmospheric CH<sub>4</sub> assume that wetland microbial sources are dominated by acetate fermentation (-58 to -65‰), and, critically, that isotopic signatures from biological sources are constant over time<sup>28,29</sup>. In contrast, we observed isotopic compositions that varied across a gradient of permafrost thaw, with hydrogenotrophic methanogenesis estimated to produce ~50–75% of total CH<sub>4</sub> emission at Stordalen (Extended Data Table 6), with  $\delta^{13}$ C averaging -80‰ (Fig. 1b). The hydrogenotrophic  $\delta^{13}$ C observed at Stordalen and other Arctic wetlands<sup>30</sup>, may be a ubiquitous characteristic of thawing permafrost, particularly during thaw stages that generate recalcitrant organic matter<sup>9,25</sup>, such as that observed here in the intermediate-thaw *Sphagnum* site.

To test whether these observed thaw-induced changes in microbial metabolism could be relevant for large-scale atmospheric methane dynamics, we used a simple box model of atmospheric mixing (Methods equation (3)) to quantify the effect of different methanogen

communities within recently constructed scenarios of CH<sub>4</sub> emission from thawing permafrost<sup>2</sup> (Extended Data Fig. 2a,b). We found that if hydrogenotrophic lineages regulate CH<sub>4</sub> isotope patterns in permafrost thaw generally, as at Stordalen, then projected CH<sub>4</sub> emissions (Fig. 3a) will produce larger reductions in δ<sup>13</sup>C of atmospheric CH<sub>4</sub> than expected from current inversion model assumptions that acetoclasts dominate emissions (Fig. 3b, Extended Data Fig. 2c,d). This, in turn would constrain our simple box model to substantially overestimate the amount of CH<sub>4</sub> released from thawing permafrost and underestimate emissions from non-wetland sources, most notably fossil fuels (Fig. 3c). The greater the prevalence of hydrogenotrophic lineages in CH<sub>4</sub> emissions, the larger will be the overestimate of fluxes from thaw (Fig 3c). The numerical size of the mis-estimation error here is illustrative; state-of-the-art 3D inversion models have spatially resolved constraints that would likely force smaller flux mis-estimation. But the general implication is that microbial effects are sufficiently important that accurate global accounting of the different sources of CH<sub>4</sub> under future climate change can be improved by understanding the microbial community dynamics underlying biological feedbacks in natural systems.

By showing that the abundance of key microbial lineages can be used to predict atmospherically relevant patterns in CH<sub>4</sub> isotopes and the proportion of carbon metabolized to CH<sub>4</sub> during permafrost thaw, this work establishes a basis for scaling changing microbial communities to ecosystem and global-scale atmospheric isotope dynamics. It also highlights the central role that microbial ecology can play in ecosystem-scale responses to global change and the benefit of incorporating microbial dynamics into earth system models.

#### 207 **References**

- Tarnocai, C. *et al.* Soil organic carbon pools in the northern circumpolar permafrost region. *Global Biogeochemical Cycles* **23**, GB2023 (2009).
- 2. Schuur, E. A. G. *et al.* Expert assessment of vulnerability of permafrost carbon to climate change. *Climatic Change* **119**, 359–374 (2013).
- 212 3. Ciais, P. et al. 2013: Carbon and Other Biogeochemical Cycles. Climate Change 2013:
- 213 The Physical Science Basis. Contribution of Working Group I to the Fifth Assesment
- 214 Report of the Intergovernmental Panel on Climate Change (2013).
- Johansson, T. *et al.* Decadal vegetation changes in a northern peatland, greenhouse gas fluxes and net radiative forcing. *Global Change Biology* **12**, 2352–2369 (2006).
- 217 5. Christensen, T. R. *et al.* Thawing sub-arctic permafrost: Effects on vegetation and methane emissions. *Geophysical Research Letters* **31**, L04501 (2004).
- Monday, R. *et al.* Discovery of a novel methanogen in thawing permafrost. *Nature Communications* (2014).doi:10.1038/ncomms4212
- 7. Melton, J. R. *et al.* Present state of global wetland extent and wetland methane modelling: conclusions from a model inter-comparison project (WETCHIMP). *Biogeosciences* **10**,
- 223 753–788 (2013).
- Jorgenson, M. T., Racine, C. H., Walters, J. C. & Osterkamp, T. E. Permafrost degradation and ecological changes associated with a warming climate in central Alaska.
   *Climate Change* 48, 551–579 (2001).
- Hodgkins, S. B. *et al.* Changes in peat chemistry associated with permafrost thaw increase greenhouse gas production. *Proceedings of the National Academy of Sciences* 111, 5819–5824 (2014).
- Olefeldt, D., Turetsky, M. R., Crill, P. M. & McGuire, A. D. Environmental and physical controls on northern terrestrial methane emissions across permafrost zones. *Global Change Biology* 19, 589–603 (2012).
- 233 11. Lee, H., Schuur, E. A. G., Inglett, K. S., Lavoie, M. & Chanton, J. P. The rate of permafrost carbon release under aerobic and anaerobic conditions and its potential effects on climate. *Global Change Biology* **18**, 515–527 (2012).
- Mackelprang, R. *et al.* Metagenomic analysis of a permafrost microbial community reveals a rapid response to thaw. *Nature* **05**, (2011).

- 238 13. Riley, W. J. et al. Barriers to predicting changes in global terrestrial methane fluxes:
- analyses using CLM4Me, a methane biogeochemistry model integrated in CESM.
- 240 *Biogeosciences* **8**, 1925–1953 (2011).
- 241 14. Koven, C. D. et al. Permafrost carbon-climate feedbacks accelerate global warming.
- 242 Proceedings of the National Academy of Sciences 108, 14769–74 (2011).
- 243 15. Turetsky, M. R., Wieder, R. K. & Vitt, D. H. Boreal peatland C fluxes under varying
- permafrost regimes. Soil Biology and Biochemistry **34**, 907–912 (2002).
- 245 16. Bäckstrand, K. et al. Annual carbon gas budget for a subarctic peatland, Northern Sweden.
- 246 *Biogeosciences* **7**, 95–108 (2010).
- 247 17. Bridgham, S. D., Cadillo-Quiroz, H., Keller, J. K. & Zhuang, Q. Methane emissions from
- 248 wetlands: biogeochemical, microbial, and modeling perspectives from local to global
- scales. *Global Change Biology* (2013).doi:10.1111/gcb.12131
- 18. Hornibrook, E. R. C. & Bowes, H. L. Trophic status impacts both the magnitude and
- stable carbon isotope composition of methane flux from peatlands. *Geophysical Research*
- 252 *Letters* **34**, 2–6 (2007).
- 253 19. Chanton, J. P., Chaser, L. C., Glaser, P. & Siegel, D. Carbon and hydrogen isotopic effects
- in microbial methane from terrestrial environments. Stable Isotopes and Biosphere-
- 255 Atmosphere Interactions, Physiological Ecolgy Series 85–105 (2005).
- 256 20. Whiticar, M. J. Carbon and hydrogen isotope systematics of bacterial formation and
- oxidation of methane. *Chemical Geology* **161**, 291–314 (1999).
- 258 21. Popp, T. J., Chanton, J. P., Whiting, G. J. & Grant, N. Methane Stable Isotope Distribution
- at a Carex Dominated Fen in North Central Alberta. Global Biogeochemical Cycles 13,
- 260 1063–1077 (1999).
- 261 22. Whiticar, M. J., Faber, E. & Schoel, M. Biogenic methane formation in marine and
- freshwater environments: CO2 reduction vs. acetate fermentation-Isotope evidence.
- 263 *Geochimica et Cosmochimica Acta* **50**, 693–709 (1986).
- 264 23. Ferry, J. G. How to make a living by exhaling methane. *Annual review of microbiology*
- **64**, 453–73 (2010).
- 266 24. Liu, Y. & Whitman, W. B. Metabolic, phylogenetic, and ecological diversity of the
- methanogenic archaea. Annals of the New York Academy of Sciences 1125, 171–89
- 268 (2008).
- 269 25. Hornibrook, E. R. C., Longstaffe, F. J. & Fyfe, W. S. Spatial distribution of microbial
- methane production pathways in temperate zone wetland soils: Stable carbon and
- hydrogen isotope evidence. *Geochimica et Cosmochimica Acta* **61**, 745–753 (1997).

- 272 26. Wania, R. et al. Present state of global wetland extent and wetland methane modelling:
- 273 methodology of a model inter-comparison project (WETCHIMP). Geoscientific Model
- 274 Development **6**, 617–641 (2013).
- 275 27. Wieder, W. R., Bonan, G. B. & Allison, S. D. Global soil carbon projections are improved
- by modelling microbial processes. *Nature Climate Change* **3**, 909–912 (2013).
- 277 28. Kai, F. M., Tyler, S. C., Randerson, J. T. & Blake, D. R. Reduced methane growth rate
- explained by decreased Northern Hemisphere microbial sources. *Nature* **476**, 194–7
- 279 (2011).
- 29. Bousquet, P. et al. Contribution of anthropogenic and natural sources to atmospheric
- 281 methane variability. *Nature* **443**, 439–43 (2006).
- 282 30. Hines, M. E., Duddleston, K. N., Rooney-Varga, J. N., Fields, D. & Chanton, J. P.
- Uncoupling of acetate degradation from methane formation in Alaskan wetlands:
- Connections to vegetation distribution. *Global Biogeochemical Cycles* **22**, 1–12 (2008).
- 285
- 286 Supplementary Information is linked to the online version of the paper at
- www.nature.com/nature.
- 288 **Acknowledgements** We thank the Abisko Scientific Research Station for infrastructure and
- logistical support, Tyler Logan and Niklas Rakos for their assistance in the field, and Steve
- Wofsy and Steve Frolking for feedback on a draft of this paper. This work was supported by the
- US Department of Energy Office of Biological and Environmental Research (award DE-
- 292 SC0004632).
- Author Contributions S.R.S., V.I.R., P.M.C., J.C. and G.W.T. designed the study. C.K.M.,
- S.B.H., R.A.W., P.M.C., J.C. and S.R.S. designed and/or performed flux/porewater/isotope
- measurements and laboratory incubations. C.K.M., B.J.W., R.M., E.-H.K., S.R.S., V.I.R. and
- 296 G.W.T. designed and/or performed analyses integrating bioinformatics and biogeochemistry.

C.K.M., V.I.R., and S.R.S wrote the paper in consultation with B.J.W., S.B.H., J.C., P.M.C., E.-H.K., R.M., and G.W.T.

**Author Information** Amplicon sequencing data have been deposited in the sequence read archive with accession number SRP042265. Reprints and permissions information is available at www.nature.com/reprints. Correspondence and requests for materials should be addressed to C.K.M (carmody.mccalley@unh.edu) or S.R.S (saleska@email.arizona.edu).

Figure 1. Increases in the magnitude and  $\delta^{13}$ C signature of CH<sub>4</sub> during permafrost thaw track shifts in methanogen communities. a, Average daily CH<sub>4</sub> emissions (error bars represent s.e.m, n = 2-3) b,  $\delta^{13}$ C composition of emitted and porewater CH<sub>4</sub> (error bars represent s.e.m, flux n = 2-3, porewater n = 6-9) and c, relative abundance of methanogenic groups as inferred by taxonomic identity assigned from 16S rRNA amplicon sequencing, for a permafrost thaw sequence at Stordalen Mire. For the intermediate thaw *Sphagnum* site, aerobic communities were sampled above the water table, anaerobic communities were sampled below the water table.

Figure 2. Correlation between the effective isotopic fractionation of methanogenesis, and both the relative abundance of the methanogen Candidatus 'Methanoflorens' stordalenmirensis', and the anaerobic  $CH_4:CO_2$  production ratio. a, The relative abundance of a single methanogen, Candidatus 'Methanoflorens stordalenmirensis' was significantly correlated (p < 0.001) with porewater effective fractionation ( $\alpha_C$ ), an isotopic indicator of methanogenic production pathway. b, Anaerobic incubations of peat collected from a related thaw sequence at Stordalen Mire (see methods in <sup>9</sup>) show a significant correlation between  $\alpha C$ 

and the CH<sub>4</sub>:CO<sub>2</sub> production ratio, suggesting that the abundance of 'M. stordalenmirensis' may be indicative of the proportion of organic matter metabolized to CH<sub>4</sub>.

321

322

323

324

325

326

327

328

329

330

331

332

333

334

335

336

337

338

339

319

320

Figure 3. Simulated effect of CH<sub>4</sub> from different methanogen communities in thawing permafrost on atmospheric δ<sup>13</sup>C-CH<sub>4</sub> in a box model of the atmosphere. a, Modeled CH<sub>4</sub> emissions under high (red bounding lines) and low (orange bounding lines) climate warming scenarios, and a range within each (in gray) spanning high and low C release scenarios<sup>2</sup>. The red dashed line is an intermediate emissions scenario used to simulate **b**, consequent reductions in δ<sup>13</sup>C of atmospheric CH<sub>4</sub> due to emissions dominated by hydrogenotrophic lineages, as in intermediate-thaw *Sphagnum* sites (green line,  $\delta^{13}C = -80\%$ ), or more by acetoclasts, as in fullythawed "Eriophorum" sites (blue line,  $\delta^{13}C = -65\%$ ). Atmospheric inversion models typically assume emissions have  $\delta^{13}$ C ranging from = -60 (black line) to -65 (blue line). (The dotted horizontal line indicates the current detection limit for atmospheric CH<sub>4</sub> isotopes<sup>28</sup>). These imply an underestimate of the effect on atmospheric  $\delta^{13}$ C for the given emissions scenario (blue or green). In order to match observed atmospheric isotopes, the box model would then require c, a corresponding overestimate of CH<sub>4</sub> flux attributed to permafrost thaw (vertical axis). The magnitude of the overestimate depends on the mismatch between model-assumed isotopic composition (upper line = -60%, lower line = -65%), and the actual isotopic composition produced by different communities, which ranges here along the horizontal axis from -80% (hydrogenotroph-dominated as in the partially-thawed "Sphagnum" sites), to -65% (acetoclastic, as in the fully thawed "Eriophorum" sites).

340

#### Methods

# Site Description and permafrost thaw

Stordalen is a sub-arctic palsa mire located 10km east of Abisko in the discontinuous permafrost zone of northern Sweden (68°21'N 18°49'E, altitude 363 m a.s.l.). This work focuses on three distinct subhabitats, common to northern wetlands and together covering ~98% of the Mire surface: (i) permafrost-dominated, well-drained palsas occupied by feather mosses and ericaceous and woody plants, covering 49% of the mire (ii) intermediate permafrost sites with variable water table depth, dominated by *Sphagnum* spp., covering 37% of the mire, and (iii) full summer-thaw, wet sites with *Eriophorum angustifolium*, covering 12% of the mire. Between 1970 and 2000, as permafrost thawed and palsas collapsed, *Sphagnum* sites and *Eriophorum* sites expanded by 3% and 54%, respectively<sup>4</sup>.

Formation of wetlands following permafrost thaw, as observed at Stordalen, is a widespread characteristic of peatlands affected by permafrost loss<sup>8,31–33</sup>. Thawing of ice-rich features results in peatland collapse and the formation bogs and fens. At Stordalen, thaw is associated with a progression from ombrotrophic bogs to minerotrophic fens due to thawinduced subsidence increasing hydrologic connectivity. A similar successional shift from bogs dominated by *Sphagnum* spp. to tall graminoid fens has been observed in other northern peatlands<sup>8,33–35</sup>. More generally, landscape features and hydrologic conditions dictate the characteristics and trajectory of wetland communities formed following permafrost thaw<sup>36</sup>. For example, rapid fen development is observed at the subsiding margins of permafrost plateaus<sup>37</sup>, whereas collapse bogs and thermokarst lakes often form within large, thawing peatland complexes<sup>32</sup>. Large uncertainty in model predictions of the extent and characteristics of wetland

formation arising from permafrost thaw is a critical limitation to current understanding of carbon-climate feedbacks<sup>7,14</sup>. As demonstrated in this study, improved characterization and modeling of peatland transformation during thaw will be essential for accurately predicting post-thaw microbial communities and the resultant magnitude and isotopic composition of CH<sub>4</sub> emissions under climate change.

#### **Methane Isotope systematics**

We use standard  $\delta$  notation for quantifying the isotopic compositions of CH<sub>4</sub> and CO<sub>2</sub>: the ratio R of  $^{13}$ C to  $^{12}$ C (or D to H) in the measured sample is expressed as a relative difference (denoted  $\delta^{13}$ C or  $\delta$ D) from the Vienna Pee Dee Belemnite (VPDB) international standard material. For example, for C:

373 
$$Q^{13}C = \frac{R - R_{VPDB}}{R_{VPDB}} = \frac{R}{R_{VPDB}} - 1 \tag{1}$$

 $\delta^{13}$ C is often expressed in parts-per-thousand (per mil, ‰).

Isotopic fractionation in chemical reactions (including methanogenesis or methanotrophy) or due to diffusion may be quantified as (Farquhar et al., 1989):

For diffusive fractionation,  $R_{source}$  is taken to be the isotopic ratio in the concentrations of the gradient and  $R_{product}$  the ratio in the resultant net flux. Because diffusion discriminates against the heavy isotope,  $R_{product} < R_{source}$ , which implies, for example, that the isotopic ratio of porewater (the "source") will be greater than that of the flux of gas diffusing out, as we see here (Fig. 1a). Methanogenesis and methanotrophy also discriminate against the heavier isotopes, so

that  $R_{product} < R_{source}$  (and hence  $\alpha > 1$ ) for both C and H in methane. Note that  $\alpha > 1$  for methanotrophy implies that the products of CH<sub>4</sub> oxidation (CO<sub>2</sub> and H<sub>2</sub>O) are lighter (have lower R) in both C and H relative to the source CH<sub>4</sub>; but mass balance then requires the residual methane not oxidized to become heavier in both C and H, relative to the starting composition of the CH<sub>4</sub> pool before oxidation.

The degree of C isotopic fractionation between  $CO_2$  and  $CH_4$  differs between the two main biochemical pathways of methanogenesis, acetoclastic ( $CH_3COOH \Rightarrow CH_4 + CO_2$ ) and hydrogenotrophic ( $CO_2 + 4H_2 \Rightarrow 2H_2O + CH_4$ ). Carbon isotope fractionation ( $\alpha_C$ ) is greater for hydrogenotrophic than for acetoclastic methanogenesis, but  $\alpha_H$  (hydrogen isotope fractionation) follows the opposite pattern:  $\alpha_H$  (hydrogenotrophic)  $< \alpha_H$  (acetoclastic) (Extended Data Fig. 1; Chanton et al<sup>19</sup>). Hence, variations in C and H isotopic compositions of  $CH_4$  that arise from variations in methanogenic pathway will be anti-correlated: shifts from hydrogenotrophic to acetoclastic production will cause C isotope ratios to increase but H isotope ratios to decline, moving along a negatively-sloped "production line" in H vs C isotope space (Extended Data Fig. 1). Isotopic variations that arise from variations in the degree of methanotrophy, by contrast, will be positively correlated: shifts towards increasing methanotrophy will cause both C and H isotope ratios to increase along a positively sloped "oxidation line" (Extended Data Fig. 1).

In a field study like this one, it is difficult to directly estimate fractionation factors directly; hence, we follow standard practice in the methane biogeochemistry literature (eg. Whiticar et al.  $^{22,38}$ ) and estimate the net or effective fractionation factor from *in situ* pore water data. For example, we estimate  $\alpha_C$ , the effective fractionation factor for C in CH<sub>4</sub>, by applying equation (2), setting  $\delta_{product} = \delta^{13}C_{CH4}$  and  $\delta_{source} = \delta^{13}C_{CO2}$ , where  $\delta^{13}C_{CH4}$  and  $\delta^{13}C_{CO2}$  are the

observed C compositions of  $CH_4$  and  $CO_2$ , respectively<sup>38</sup>. Using  $CO_2$  isotope composition for  $\delta_{source}$  follows directly for hydrogenotrophic methanogenesis (for which  $CO_2$  is the source C substrate), and has been found to work also in practice for acetoclastic methanogenesis, as porewater  $CO_2$  arises primarily from respiration of organic matter (a non-discriminatory reaction), and so is typically isotopically indistinguishable from organic matter<sup>20,39</sup>.

411

412

413

414

415

416

417

418

419

420

421

422

423

424

425

426

427

428

406

407

408

409

410

#### **Autochamber measurements**

The autochamber system at Stordalen mire has previously been described in detail for measurements of CO<sub>2</sub> and total hydrocarbons <sup>16,40</sup>. Briefly, a system of 8 automatic gas-sampling chambers made of transparent Lexan was installed in the three habitat types at Stordalen Mire in 2001 (n=3 each in the palsa and *Sphagnum* habitats, and n=2 in the *Eriophorum* habitat). Each chamber covers an area of 0.14 m<sup>2</sup> (38 cm x 38 cm), with a height of 25–45 cm, and is closed once every 3 hours for a period of 5 min. The chambers are connected to the gas analysis system, located in an adjacent temperature controlled cabin, by 3/8" Dekoron tubing through which air is circulated at approximately 2.5 L min<sup>-1</sup>. During the 2011 season the system was updated with a new chamber design similar to that described by Bubier et al<sup>41</sup>. The new chambers each cover an area of 0.2 m<sup>2</sup> (45 cm x 45 cm), with a height ranging from 15-75 cm depending on habitat vegetation. At the Palsa and Sphagnum site the chamber base is flush with the ground and the chamber lid (15 cm in height) lifts clear of the base between closures. At the *Eriophorum* site the chamber base is raised 50–60 cm on lexon skirts to accommodate large stature vegetation. Additionally, each chamber is instrumented with thermocouples measuring air and surface ground temperature, and water table depth is measured manually 3–5 times per week. The Palsa site chambers are located within the palsa site in Monday, Woodcroft et al<sup>6</sup> and correspond to the hummock site class (I) described in Johansson et al<sup>4</sup>. The *Sphagnum* site chambers are located within the bog site in Monday, Woodcroft et al<sup>6</sup> or site S in Hodgkins et al<sup>9</sup> and correspond to the semi-wet and wet site class (II and III) described in Johansson et al<sup>4</sup>. The *Eriophorum* site chambers are located within the fen site in Monday, Woodcroft et al<sup>6</sup> or site E in Hodgkins et al<sup>9</sup> and correspond to the tall graminoid site class (IV) described in Johansson et al<sup>4</sup>.

## **QCLS** measurement and calibration

Methane fluxes and isotopes were measured using a Quantum Cascade Laser Spectrometer (QCLS, Aerodyne Research Inc), deployed to Stordalen Mire in June 2011. The QCLS instrument deployed at Stordalen is a modification of the technology described in detail by Santoni et al<sup>42</sup>. Briefly, the QCLS uses a room-temperature continuous wave mid-infrared laser whose frequency was tuned to rapidly (900 kHz) scan across  $^{12}$ CH<sub>4</sub> and  $^{13}$ CH<sub>4</sub> absorption lines in the 7.5 µm region. The laser light enters a multipass sample cell (effective path length of ~200m) containing sample air at low pressure (~5 kPa) and is detected by a thermoelectrically cooled detector (no cryogens are needed). Aerodyne Research's custom TDL Wintel software averages high-frequency spectra to produce independent  $^{12}$ CH<sub>4</sub> and  $^{13}$ CH<sub>4</sub> mixing ratios in the sample airstream at 1 sec intervals. The ratio, R, of  $^{13}$ CH<sub>4</sub> to  $^{12}$ CH<sub>4</sub> and can then be expressed in standard notation as  $\delta^{13}$ C, the part-per-thousand (per mil, ‰) deviation of the measured ratio from the VPDB standard  $^{13}$ C/ $^{12}$ C ratio  $R_{VPDB}$ , according to equation (1).

Instrument precision in the field at Stordalen Mire was assessed using time-series measurements of calibration tank air over 30–40 min. The precision of  $\delta^{13}$ C CH<sub>4</sub> measurements using a 1 second integration time was 1‰. The Allan variance technique (used to characterize the minimum possible measurement error and the averaging time required to achieve it<sup>43</sup>),

showed that the minimum measurement error on  $\delta^{13}\text{C-CH}_4$  was <0.2%, achieved with 60 seconds of averaging time. This approaches the precision of comparable measurements made using GC-IRMS.

We connected the QCLS to the main autochamber circulation using ½" Dekoron tubing and a solenoid manifold that enables selection between the autochamber flow and an array of calibration tanks. During measurement periods, filtered (0.45 µm, Teflon filter) and dried (Perma Pure PD-100T-24MSA) sample-air flows at 1.4 slpm through the 2L QCLS sample cell volume at 5.6 kPa. A downstream solenoid controls the QCLS return flow so that air only recirculates during autochamber measurement periods, during calibration periods exhaust air is vented to the room.

Calibrations were done every 60 min using 3 calibration gases spanning the observed concentration range (1.5–10 ppm). The CH<sub>4</sub> concentration and  $\delta^{13}$ C composition of each calibration tank was determined by inter-calibration with a set of 4 well-characterized primary standard tanks. The primary tanks (Scott Marin, Inc, Riverside CA) were calibrated to the VPDB scale by means of flask samples, which were analyzed by GC-IRMS at Florida State University (see porewater methods for GC-IRMS details). Each isotopologue, <sup>12</sup>CH<sub>4</sub> and <sup>13</sup>CH<sub>4</sub>, was treated as an independent measurement and calibrated separately. For each calibration period a linear calibration curve was fitted for each isotopologue and the fit parameters were then linearly interpolated between calibration periods. The interpolated fit parameters were applied to the measured sample isotopologue mixing ratios to give calibrated measurements of <sup>12</sup>CH<sub>4</sub>, <sup>13</sup>CH<sub>4</sub>, and total CH<sub>4</sub>, from which  $\delta^{13}$ C-CH<sub>4</sub>, was calculated.

#### **Autochamber data processing**

For each autochamber closure we calculated flux and  $\delta^{13}$ C signiture of emitted CH<sub>4</sub>. Fluxes were calculated using a method consistent with that detailed by Bäckstrand et al<sup>44</sup> for CO<sub>2</sub> and total hydrocarbons, using a linear regression of changing headspace CH<sub>4</sub> concentration over a period of 2.5 min. Eight 2.5 min regressions were calculated, staggered by 15 sec, and the most linear fit (highest r<sup>2</sup>) was then used to calculate flux. Keeling plots 45-47 using the entire closure period were used to estimate the isotopic composition of the emitted CH<sub>4</sub>. As demonstrated by Santoni et  $al^{42}$ , negligible error in measurment of CH<sub>4</sub> relative to that of  $\delta^{13}$ CH<sub>4</sub> for this instrumentation meant that Type I regression was sufficient for the Keeling plot analysis. When the total change in headspace CH<sub>4</sub> was low 45, there was high error in the Keeling intercept. We used a threshold of 3% uncertainty in the Keeling intercept as a cut-off for including isotopic values in the calculation of daily and annual averages, resulting in a total of 1569 observations at the Sphagnum site and 1168 at the Eriophorum site. No Palsa chamber closures had sufficient  $CH_4$  flux to calculate  $\delta^{13}CH_4$ . Daily and whole-season average flux and isotopic composition for each habitat were calculated based on individual chambers as the unit of replication (n=3 for Palsa and Sphagnum, n=2 for Eriophorum). Significant differences in the magnitude and isotopic composition of CH<sub>4</sub> emissions were determined using a Student's t-test (isotopic composition) and ANOVA (flux magnitude) in R<sup>48</sup>, with seasonal averages for each auto-chamber as the unit of replication. Statistical significance was determined at  $\alpha = 0.05$ .

#### Porewater sampling and analysis

473

474

475

476

477

478

479

480

481

482

483

484

485

486

487

488

489

490

491

492

493

494

495

Porewater samples were collected on July 12, 2011, August 15, 2011 and October 15, 2011 at three locations adjacent to the *Sphagnum* and *Eriophorum* auto-chamber sites (Extended Data Table 1). Samples were collected by suction with a syringe through a stainless steel tube and filtered through 25-mm diameter Whatman Grade GF/D glass microfiber filters (2-µm

particle retention). Porewater pH was measured in the field (Oakton Waterproof pHTestr 10, Eutech Instruments). Samples for the analysis of the concentration and  $\delta^{13}$ C of CH<sub>4</sub> and CO<sub>2</sub> were injected into 30-mL evacuated vials sealed with butyl rubber septa and frozen within 8 hours of collection. The samples for  $\delta$ D-CH<sub>4</sub> were injected into 120-mL evacuated vials sealed with butyl rubber septa and containing 0.5 g of KOH. For  $\delta$ D-H<sub>2</sub>O, water was filtered directly into 2-mL plastic screw cap vials so that the vials were completely filled, then frozen within 8 hours of collection. All samples were shipped frozen to Florida State University for analysis.

Samples collected for analysis of  $CH_4$  and  $CO_2$  concentrations and  $\delta^{13}C$  were thawed, acidified with 0.5 mL of 21%  $H_3PO_4$ , and brought to atmospheric pressure with helium. The sample headspace was analyzed for concentrations and  $\delta^{13}C$  of  $CH_4$  and  $CO_2$  on a continuous-flow Hewlett-Packard 5890 gas chromatograph (Agilent Technologies) at  $40^{\circ}C$  coupled to a Finnigan MAT Delta S isotope ratio mass spectrometer via a Conflo IV interface system (Thermo Scientific, Bremen, Germany). The headspace gas concentrations were converted to porewater concentrations based on their known extraction efficiencies, defined as the proportion of formerly-dissolved gas in the headspace. An extraction efficiency of 0.95 (based on repeated extractions) was used for  $CH_4$ , and the extraction efficiency for  $CO_2$  relative to DIC was determined based on  $CO_2$  extraction from dissolved bicarbonate standards<sup>49</sup>.

Samples collected for analysis of  $\delta D$ -CH<sub>4</sub> were brought to atmospheric pressure with helium and measured on a gas chromatograph connected to a ThermoFinnegan Delta Plus continuous flow isotope ratio mass spectrometer at the National High Magnetic Field Laboratory (Tallahassee, FL).  $\delta D$  of CH<sub>4</sub> is affected by  $\delta D$  of H<sub>2</sub>O because CH<sub>4</sub> exchanges H atoms with water during methanogenesis  $^{20,38,50}$ , so measurement of  $\delta D$ -H<sub>2</sub>O is necessary for correct

assignment of  $CH_4$  production mechanisms and oxidation based on  $\delta D$  and  $\delta^{13}C$  of  $CH_4$ . Samples collected for  $\delta D$ - $H_2O$  were measured on an LGR DT-100 liquid water stable isotope analyzer at Florida Agricultural and Mechanical University (Tallahassee, FL). Data analysis for these samples was performed using an MS Excel template from the IAEA Water Resources Programme (<a href="http://www.iaea.org/water">http://www.iaea.org/water</a>).

Significant differences in  $\alpha_C$  and  $\delta D$  and  $\delta^{13}C$  of porewater  $CH_4$  between the *Sphagnum* and *Eriophorum* sites were determined using a Student's t-test ( $\alpha_C$ ,  $\delta D$ - $CH_4$ ,  $\delta^{13}C$ - $CH_4$ ) and Hotelling's t-test (multivariate  $\delta D$  and  $\delta^{13}C$  of  $CH_4$ ) in  $R^{48}$ . Statistical significance was determined at  $\alpha=0.05$ .

## **Peat sampling**

Peat samples were collected on July 12, 2011, August 16, 2011 and October 16, 2011 at three locations adjacent to the Palsa, *Sphagnum* and *Eriophorum* auto-chamber sites. For the *Sphagnum* and *Eriophorum* sites samples were collected at the same depths and locations used for porewater sampling (Extended Data Table 1), sample depths for the Palsa site are detailed in Mondav et al<sup>6</sup>. Peat cores were collected using a 11 cm diameter push corer (Palsa and *Sphagnum* sites) or a 10 cm x 10 cm Wardenaar corer (*Eriophorum* site). Cores were subsampled by depth and were subdivided in the field for microbial and chemical analysis, avoiding the outer 1cm of the core. Samples for microbial analysis were placed in cryotubes, saturated with ~3 volumes LifeGuard solution (MoBio Laboratories, Carlsbad, CA, USA) and stored at -80°C until processing. Samples for chemical analysis were placed in plastic bags and frozen until

#### **Peat chemical analysis**

For peat %C, %N, C:N ratio, and  $\delta^{13}$ C measurements, 5–10 g of peat was dried at 60 °C until completely dry (3–10 days) and ground to a fine powder. Subsamples of ground peat (80–100 µg for %C and  $\delta^{13}$ C analysis, and 5000–6000 µg for %N analysis) were wrapped in tin capsules and analyzed by combustion to CO<sub>2</sub> and N<sub>2</sub> at 1020 °C in an automated CHN elemental analyzer coupled with a ThermoFinnegan Delta XP isotope ratio mass spectrometer at the National High Magnetic Field Laboratory (Tallahassee, FL). Samples were run in non-dilution mode for carbon analysis and dilution mode (×10) for nitrogen analysis. C:N was calculated as the ratio of (%C)/(%N) (by weight) for corresponding pairs of subsamples.

### SSU rRNA gene amplicon analysis

Sampling and extraction was carried out as per Mondav et al <sup>6</sup>. Several additional samples were analyzed for this paper, multiplex identifiers for those runs not reported in Mondav et al <sup>6</sup> are provided in Extended Data Table 7. SSU rRNA gene sequences were processed using APP 3.0.3 (https://github.com/Ecogenomics/APP). Homoploymer errors were corrected using Acacia <sup>51</sup> and the resulting reads were processed using the CD-HIT-OTU 0.0.2 pipeline with minor adjustments <sup>52</sup>. All reads were trimmed to 250bp and reads <250bp were discarded.

Sequences were clustered at 97% identity and each cluster assigned a taxonomy using BLASTN 2.2.22 <sup>53</sup> through the QIIME script assign\_taxonomy.py <sup>54</sup> against the GreenGenes Oct 2012 database clustered at 99% identity (Supplementary Data 1). Each abundant methanogenic cluster's taxonomy was confirmed using parsimony insertion with ARB <sup>55</sup> Amplicon sequence clusters were identified as potential hydrogenotrophic or acetoclastic methanogens based on taxonomic relationship to known methanogenic lineages (Extended Data Table 2)<sup>23,24,56</sup>. Within

the order *Methanosarcinales*, lineages most closely related to *Methanosaeta* were classified as obligate acetoclasts, whereas those most closely related to *Methanosarcina* were considered facultative acetoclasts, having the potential for both acetoclastic or hydrogenotrophic production<sup>23</sup>.

568

569

570

571

572

573

574

575

576

577

578

579

580

581

582

583

584

585

586

564

565

566

567

#### **Regression analysis**

A step-wise regression approach using Akaike's information criterion (AIC) as the model selection criterion was used to identify a sub-set of microbial and environmental predictor variables that best explained CH<sub>4</sub> metabolism patterns quantified as porewater  $\alpha_C$  (Extended Data Table 5). Model selection was done using the stepAIC package in R and the relative importance of the predictor variables in the selected model was then calculated using the relaimpo R package <sup>48</sup>. Variables included in the model selection process included the relative abundance of the 6 most abundant methanogen operational taxonomic units (OTUs) (comprising >93% of total methanogen sequences; see Extended Data Table 2) plus soil temperature, water table depth, pH, porewater CH<sub>4</sub> and DIC concentration, and peat C:N, % C, % N and δ<sup>13</sup>C (Extended Data Table 1). Strong correlation between pH and both water table depth and peat  $\delta^{13}$ C as well as peat %N and both %C and C:N meant that pH and %N were excluded from the regression analysis. Removing non-significant predictor variables (DIC and relative abundance of an unidentified Methanobacterium spp. (otu-3636, Extended Data Table 2)) had a minimal effect on the model AIC value (<1) and this simplified version was therefore selected as the optimal model (Model 2 in Extended Data Table 5). Stepwise regression was also done with  $\delta^{13}$ C-CH<sub>4</sub> as the dependent variable. This analysis resulted in a similar model outcome, but with a lower R<sup>2</sup> (Model 1 in Extended Data Table 8). Stepwise regression analysis with environmental predictor variables and the relative abundance of the influential methanogen 'M stordalenmirensis' (otu-10747) as the dependent variable showed that patterns in this methanogen's abundance were influenced by environmental conditions, particularly water table depth and peat chemistry (Model 2 in Extended Data Table 8). These environmental variables alone, however, cannot fully replace microbial data when modeling  $\alpha_C$ . Stepwise regression analysis using only environmental variables to predict  $\alpha_C$  yielded a model with a lower AIC and  $R^2$  (Model 3 in Extended Data Table 8). It is the combination of methanogen and environmental variables that yields a model that explains the most variability in  $\alpha_C$  (Extended Data Table 5).

# **Box Model of atmospheric methane**

The model used here was a 1-box model simplified from the 2-box model of Tans<sup>57</sup> (and also used in the Kai et al.<sup>28</sup> methane inversion study):

$$\frac{dM}{dt} = F_{CH_4} - /M$$

$$\frac{d(RM)}{dt} = R_{CH_4} F_{CH_4} - \alpha_{OH} \lambda (RM)$$
(3)

where M is the mixing ratio (in ppbv) of CH<sub>4</sub> in the atmosphere,  $F_{CH4}$  is the source flux of CH<sub>4</sub> to the atmosphere,  $\lambda$  is atmospheric removal rate (1/9 yr<sup>-1</sup>, assumed for this illustration to be fixed), the R terms are the ratio of  $^{13}$ CH<sub>4</sub> to  $^{12}$ CH<sub>4</sub>, as defined for equation (1), and  $\alpha_{OH}$  is the isotopic fractionation (= 0.994, or about -6‰) for atmospheric oxidation of CH<sub>4</sub> by OH<sup>28</sup>. Baseline flux to the atmosphere ( $F_{CH4}$ ) was set to 559 Tg CH<sub>4</sub> the 1980 value<sup>28</sup>. The isotopic composition of CH<sub>4</sub> inputs to the atmosphere ( $R_{CH4}$ ) were set to the equivalent of -53‰ to allow steady-state modern atmospheric CH<sub>4</sub> to have the observed value of ~ -47‰.

We implemented this model numerically in the R software package<sup>48</sup>, simulating the effect on the atmosphere of CH<sub>4</sub> emission due to permafrost thaw and partial decomposition of the 1,700 PgC stock of permafrost C anticipated over the next 300 years, as summarized in Schurr et al<sup>2</sup> and Tarnocai et al<sup>1</sup>. High and low permafrost carbon release scenarios for both high (IPCC scenario RCP8.5, leading to release of 120 to 195 PgC) and low (IPCC scenario RCP2.6, approximated as one-third the C release of the high scenario) climate change scenarios (Extended Data Fig. 2a) generated CH<sub>4</sub> emissions (Fig. 3a) (based on 2.3% of released permafrost carbon emerging as CH<sub>4</sub>. Schurr et al<sup>2</sup>) and corresponding impacts on the atmospheric concentrations of CH<sub>4</sub> (Extended Data Fig. 3b). We simulated the impacts of these emissions on the isotopic composition of atmospheric CH<sub>4</sub> by assuming the  $\delta^{13}$ C of CH<sub>4</sub> emitted was in the range of what we report here for Stordalen Mire, from very light (-80%, like that measured in the Sphagnum site) to only moderately light (-65‰, like that measured in the Eriophorum site), giving a range of isotopic perturbations to atmospheric CH<sub>4</sub> under high climate change (Extended Data Fig. 2c) and under low climate change (Extended Data Fig. 2d). In all scenarios, the induced change in atmospheric  $\delta^{13}$ C is significantly larger than the atmospheric detection limit of 0.1% (reported in Kai et al <sup>28</sup> and shown as a dotted horizontal line in Extended Data Fig. 3c,d). For the analysis shown in Fig. 3, we focused on a mid-range value of permafrost C

607

608

609

610

611

612

613

614

615

616

617

618

619

620

621

622

623

624

625

626

627

628

629

release (high climate change scenario with low C release, 120 Pg total C by 2100), corresponding to emissions of 2.8 PgC as CH<sub>4</sub> by 2100 (the dashed black-and-red line in Fig. 3a). (By comparison, the IPCC estimates that up to 5 PgC may be released as CH<sub>4</sub> by 2100.<sup>3</sup>) We explored the mis-attribution of C release that would occur by (mistakenly) assuming that isotopic composition of emitted CH<sub>4</sub> was in the range of assumptions used in previous

- atmospheric inversions, from -60% to -65% <sup>28</sup>, instead of the range measured at Stordalen Mire
- 631 (-65‰ to -80‰). We estimated the magnitude of mis-attribution (or error flux, Fig. 3c) by
- simulating the amount of additional carbon that would need to be released (at nominally assumed
- 633 isotopic composition values of -60 or -65) in order to have the same effect on atmospheric
- composition as the carbon released under scenarios with isotopic compositions like those
- observed in the field.

636

637

#### References

- 638 31. Payette, S. Accelerated thawing of subarctic peatland permafrost over the last 50 years. *Geophysical Research Letters* **31**, 1–4 (2004).
- 640 32. O'Donnell, J. a. *et al.* The Effects of Permafrost Thaw on Soil Hydrologic, Thermal, and Carbon Dynamics in an Alaskan Peatland. *Ecosystems* **15**, 213–229 (2012).
- Vitt, D. H., Halsey, L. A. & Zoltai, S. C. The changing landscape of Canada's western
   boreal forest: the current dynamics of permafrost. *Canadian Journal of Forest Research* 30, 283–287 (2000).
- Quinton, W. L., Hayashi, M. & Chasmer, L. E. Permafrost-thaw-induced land-cover change in the Canadian subarctic: implications for water resources. *Hydrological Processes* 25, 152–158 (2011).
- Zoltai, S. C. Cyclic Development of Permafrost in the Peatlands of Northwestern Alberta,
   Canada. Arctic and Alpine Research 25, 240–246 (1993).
- 650 36. Camill, P. & Clark, J. S. Climate change disequilibrium of boreal permafrost peatlands caused by local processes. *The American naturalist* **151**, 207–222 (1998).
- Dyke, L. D. & Sladen, W. E. Permafrost and Peatland Evolution in the Northern Hudson
   Bay Lowland, Manitoba. *Arctic* 63, 429–441 (2010).
- Whiticar, M. J. & Faber, E. Methane oxidation in sediment and water column environments Isotopic evidence. *Organic Geochemistry* **10**, 759–768 (1986).
- 656 39. Conrad, R. Quantification of methanogenic pathways using stable carbon isotopic signatures: a review and a proposal. *Organic Geochemistry* **36**, 739–752 (2005).

- 40. Bäckstrand, K., Crill, P. M., Mastepanov, M., Christensen, T. R. & Bastviken, D. Nonmethane volatile organic compound flux from a subarctic mire in Northern Sweden. *Tellus* 660 B 60, 226–237 (2008).
- 661 41. Bubier, J. L., Crill, P. M., Mosedale, A., Frolking, S. & Linder, E. Peatland responses to varying interannual moisture conditions as measured by automatic CO<sub>2</sub> chambers. *Global Biogeochemical Cycles* **17**, (2003).
- 664 42. Santoni, G. W. *et al.* Mass fluxes and isofluxes of methane (CH<sub>4</sub>) at a New Hampshire fen 665 measured by a continuous wave quantum cascade laser spectrometer. *Journal of* 666 *Geophysical Research* **117**, D10301 (2012).
- Werle, P., Mücke, R. & Slemr, F. The Limits of Signal Averaging in Atmospheric Trace Gas Monitoring by Tunable Diode-Laser Absorption Spectroscopy (TDLAS). *Applied Physics B* 139, 131–139 (1993).
- 44. Bäckstrand, K., Crill, P. M., Mastepanov, M., Christensen, T. R. & Bastviken, D. Total
   hydrocarbon flux dynamics at a subarctic mire in northern Sweden. *Journal of Geophysical Research* 113, (2008).
- 673 45. Pataki, D. E. The application and interpretation of Keeling plots in terrestrial carbon cycle research. *Global Biogeochemical Cycles* **17**, (2003).
- 675 46. Keeling, C. D. The concentration and isotopic abundances of atmospheric carbon dioxide in rural areas. *Geochimica et Cosmochimica Acta* **13**, 322–334 (1958).
- 677 47. Keeling, C. D. The concentration and isotopic abundances of carbon dioxide in rural and marine air. *Geochimica et Cosmochimica Acta* **24**, 277–298 (1960).
- 48. Team, R. C. R: A language and environment for statistical computing. R Foundation for Statistical Computing. ISBN 3–900051–07–0 (2012).at <a href="http://www.r-project.org/">http://www.r-project.org/</a>
- 681 49. Corbett, J. E. *et al.* Partitioning pathways of CO<sub>2</sub> production in peatlands with stable carbon isotopes. *Biogeochemistry* **114**, 327–340 (2013).
- 683 50. Chanton, J. P., Fields, D. & Hines, M. E. Controls on the hydrogen isotopic composition 684 of biogenic methane from high-latitude terrestrial wetlands. *Journal of Geophysical* 685 *Research* 111, 1–9 (2006).
- Bragg, L., Stone, G., Imelfort, M., Hugenholtz, P. & Tyson, G. W. Fast, accurate errorcorrection of amplicon pyrosequences. *Nature Methods* **9**, 425–426 (2012).
- Li, W. & Godzik, A. Cd-hit: a fast program for clustering and comparing large sets of proteins or nucleotide sequences. *Bioinformatics* **22**, 1658–1659 (2006).

- 690 53. Altschul, H. J. *et al.* Gapped BLAST and PSI-BLAST: A new generation of protein database search programs. *Nucleic Acids Research* **25**, 3389–3402 (1997).
- 692 54. Caporaso, J. G. *et al.* QIIME allows analysis of high-throughput community sequencing data. *Nature Methods* **7**, 335–336 (2010).
- 55. Ludwig, W. *et al.* ARB: a software environment for sequence data. *Nucleic Acids Research* **32**, 1363–71 (2004).
- 696 56. Conrad, R. The global methane cycle: recent advances in understanding the microbial processes involved. *Environmental Microbiology Reports* **1**, 285–292 (2009).
- 57. Tans, P. P. A note on isotopic ratios and the global atmospheric methane budget. *Global Biogeochemical Cycles* **11**, 77–81 (1997).

#### **Total** 701 Extended Data Figure and Table Legends:

Extended Data Figure 1. Expected and observed relationships between  $\delta D$  and  $\delta^{13}C$  content of porewater CH<sub>4</sub>. The thick gray arrow shows the expected pattern in H and C isotopes of CH<sub>4</sub> when variations are caused by shifts between acetoclastic (lower right) and hydrogenotrophic (upper left) production. The thin black arrows pointing to the upper right indicate the expected pattern in H and C isotopes of CH<sub>4</sub> when variations are caused by changes in CH<sub>4</sub> oxidation<sup>19</sup>. The points are observed isotopic compositions of samples collected July–October 2011 at the partly thawed *Sphagnum* and fully thawed *Eriophorum* sites, with site averages shown with error bars (error bars represent s.e.m, n = 13 (*Sphagnum*) and 20 (*Eriophorum*)). Although the scatter allows for some variation in both production and oxidation, the average *Eriophorum* porewater CH<sub>4</sub> had significantly more <sup>13</sup>C and less D relative to *Sphagnum* porewater (Hotelling's T<sup>2</sup> Test, p = 0.0001), indicating that overall inter-site isotopic differences were due mostly to differences in CH<sub>4</sub> production pathway rather than to differences in CH<sub>4</sub> oxidation. Additionally, in August there was also a significant, negative relationship between  $\delta^{13}$ C-CH<sub>4</sub> and  $\delta$ D-CH<sub>4</sub> of porewater samples collected across sites (dashed line, R<sup>2</sup> = 0.5, p < 0.02). Note that on the vertical axis,

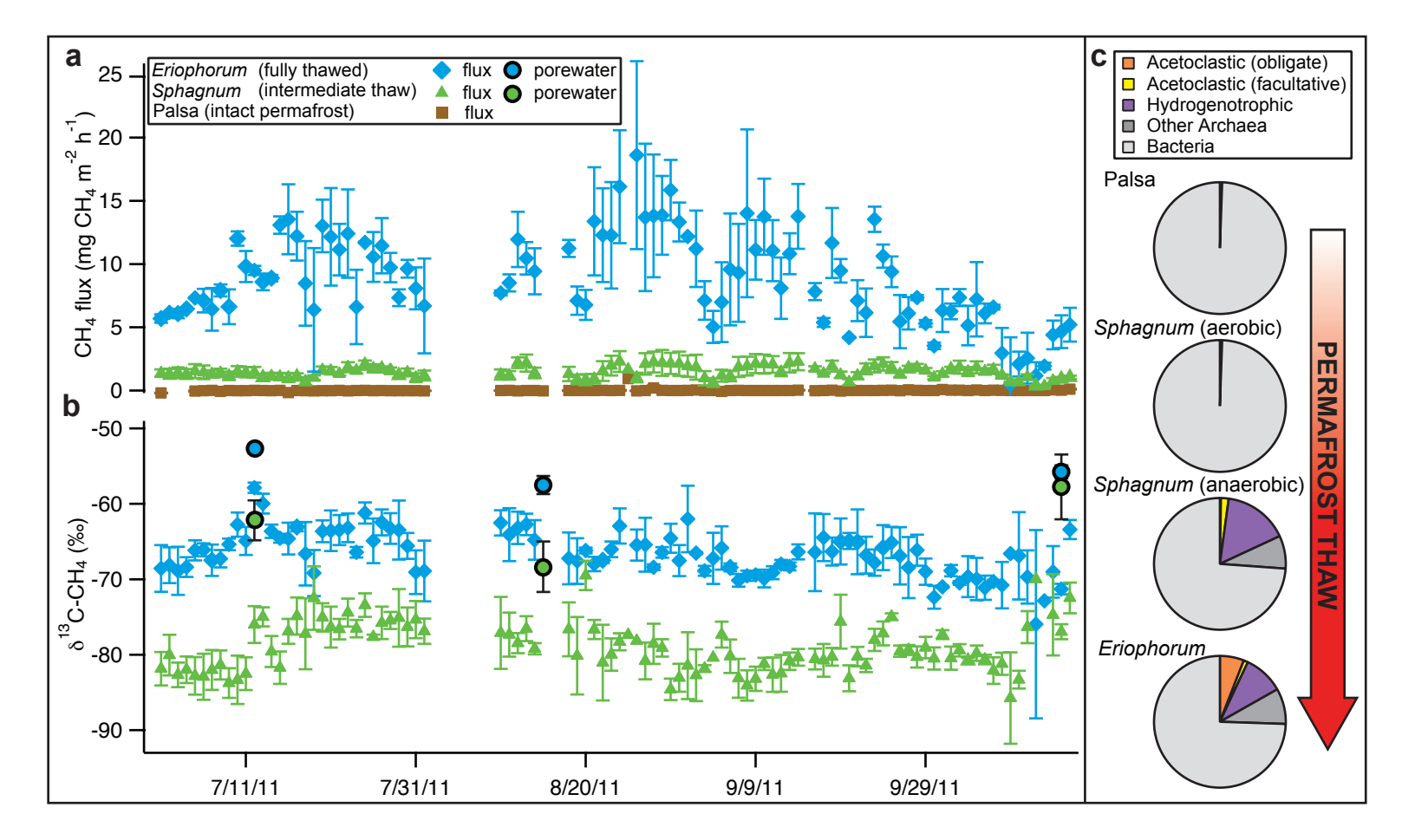
716  $\delta D$ -H<sub>2</sub>O has been subtracted from  $\delta D$ -CH<sub>4</sub> to correct for the effect of  $\delta D$  exchange between H<sub>2</sub>O and CH<sub>4</sub> <sup>20,38,50</sup>. 717 718 719 Extended Data Figure 2. Simulations, using high and low temperature and C release 720 scenarios, of the effect of CH<sub>4</sub> release from thawing permafrost on atmospheric  $\delta^{13}$ C-CH<sub>4</sub>. 721 a, Scenarios of permafrost C release due to thaw (high temperature, red bounding lines; low 722 temperature, orange bounding lines; with the range in each case defined by high and low C-723 release scenarios); b, Impact on atmospheric methane mixing ratios (assuming 2.3% of released 724 C is emitted as methane); c, Impact of high climate change scenario on atmospheric methane isotopes, assuming "Eriophorum-like" emissions ( $\delta^{13}$ C  $\approx$  -65%, blue bounding lines), or 725 assuming "Sphagnum-like" emissions ( $\delta^{13}$ C  $\approx$  -80%, green bounding lines); and **d**, Same as (c), 726 727 except for low climate change scenario. In (c) and (d) dotted horizontal lines indicate the detection limit for CH<sub>4</sub> isotopes <sup>28</sup>. 728 729 730 Extended Data Table 1. Summary of porewater chemistry, average (standard error), n=3. 731 732 Extended Data Table 2. Relative abundance, taxonomic classification and predicted 733 methanogenic pathway of the dominant methanogen operational taxonomic units (OTUs). 734 735 Extended Data Table 3. Relative abundance of methanogen functional groups within 736 the Archaea 737 \*Above the water table 738 †Below the water table

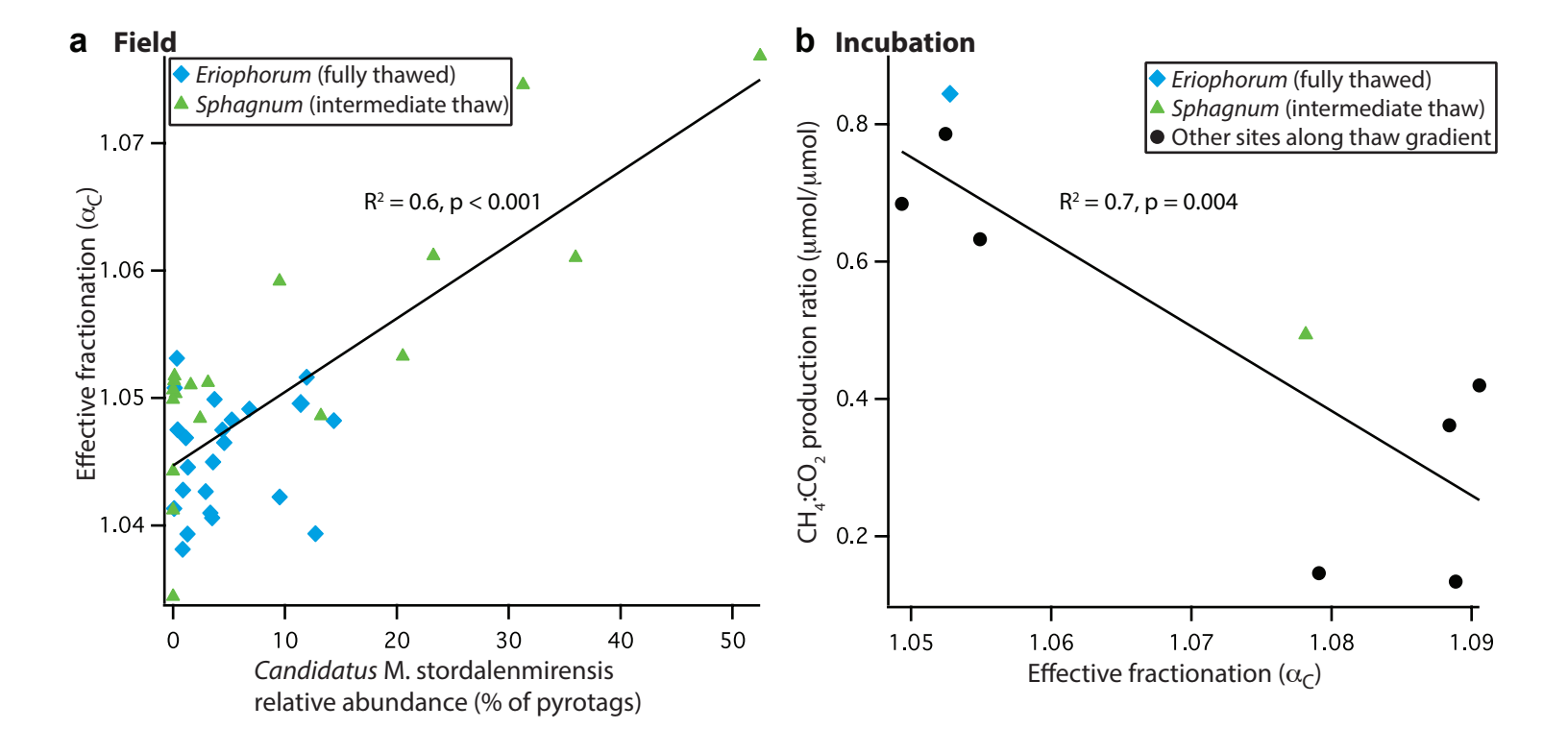
/39	
740	Extended Data Table 4. Results of linear regression analysis for predicting $\alpha_{\text{C}}$ from
741	relative abundances of methanogenic pathways, dominant methanogenic lineages
742	and environmental variables (n = 41)
743	*see Extended Data Table 2 for taxonomic details
744	
745	Extended Data Table 5. Results of stepwise multiple regression analysis for
746	predicting $\alpha_{\text{C}}$ from relative abundances of methanogenic lineages and environmenta
747	variables
748	*see Extended Data Table 2 for taxonomic details
749	
750	Extended Data Table 6. Estimate of the relative contribution of hydrogenotrophic
751	production to annual CH <sub>4</sub> emission at Stordalen mire
752	* Based on Johansson et al. 4, the <i>Sphagnum</i> site in this study is representative of the
753	Semiwet and Wet vegetation classes.
754	$^\dagger Annual total hydrocarbon emissions from Bäckstrand et al. ^{16}$ corrected for non-methane
755	volatile organic compound (NMVOC) flux using the reported proportions (25% NMVOC for
756	the $\it Eriophorum$ site, 15% for the $\it Sphagnum$ site). The magnitude of growing season $\it CH_4$
757	emissions measured in this study is comparable to the growing season CH <sub>4</sub> flux used in the
758	Bäckstrand et al. estimate of annual flux.
759	$^{\ddagger} Two \ approaches: \ isotopic, using mixing of acetoclastic (-60%) and hydrogenotrophic (-$
760	80‰) sources to yield mean emitted $\delta^{13}\text{C-CH}_4\text{,}$ and molecular, using proportion of the
761	methanogen community identified as hydrogenotrophic.

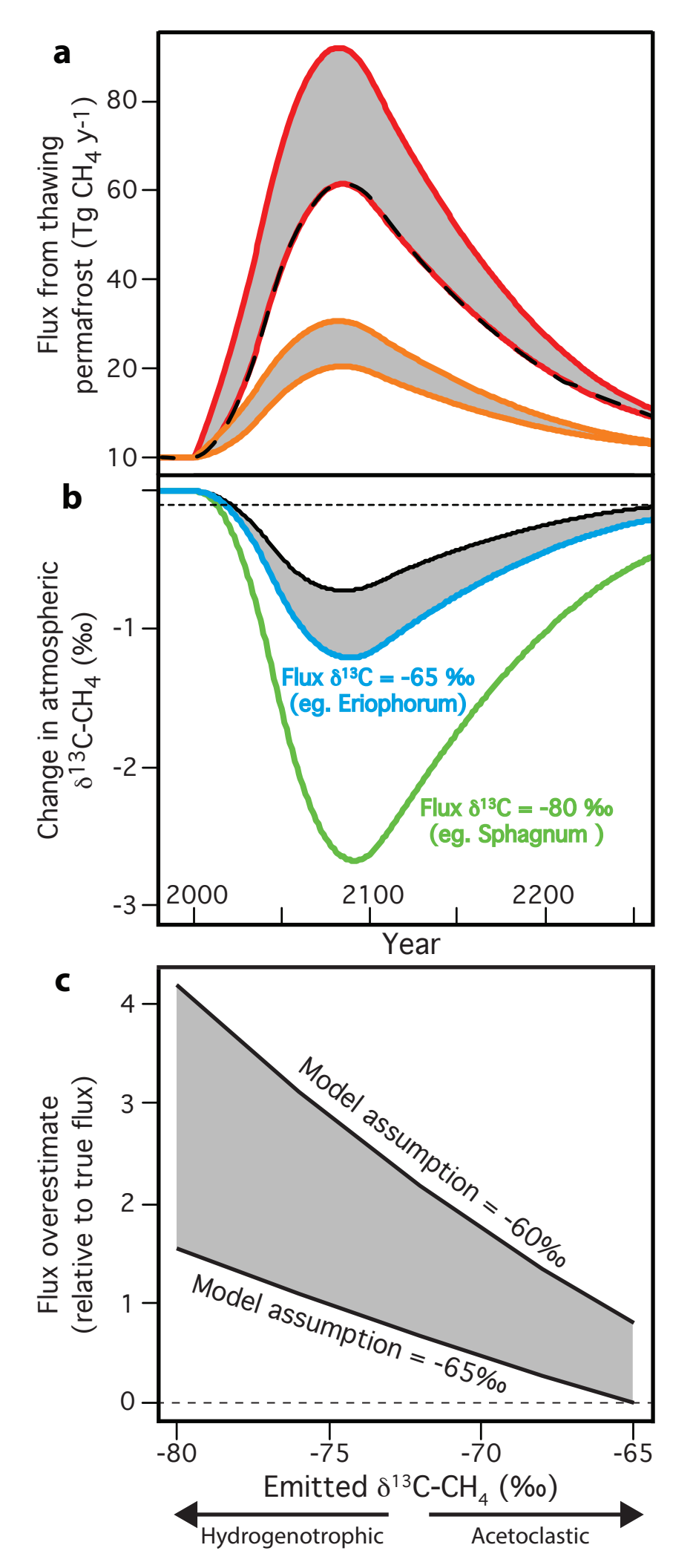
762 § Molecular approach: on average 86% of methanogen community in the anoxic CH<sub>4</sub>-763 producing peat was identified as hydrogenotrophic, all of the acetoclasts were facultative 764 so this is likely an underestimation of potential hydrogenotrophic production. 765 || Isotopic approach:  $-79.6\%_0 \sim -80\%_0 * 0.98 + -60\%_0 * 0.02$ ¶Isotopic approach:  $-66.3\% \sim -80\% * 0.32 + -60\% * 0.68$ 766 <sup>#</sup> Molecular approach: on average 62% of the methanogen community was identified as 767 768 hydrogenotrophic. 769 770 Extended Data Table 7. SSU rRNA gene amplicon multiplex identifiers (MIDs) used for 771 each sample 772 \* Sample names are comprised of the date of sampling, followed by P, S or E for Palsa, 773 Sphagnum, or Eriophorum sites, respectively, the number indicates the core within the site, and 774 S, M or D indicates surface, middle or deep sampling within the core, respectively. 775 † Samples were multiplexed in six separate runs, each time with samples not related to this study. 776 The multiplex identifiers of the first five runs are given in Monday et al <sup>6</sup>. 777 778 Extended Data Table 8. Results of stepwise multiple regression analysis for predicting 779 δ<sup>13</sup>C-CH<sub>4</sub> from relative abundances of methanogenic lineages and environmental variables 780 (Model 1), the relative abundance of 'M. stordalenmirensis' from environmental variables

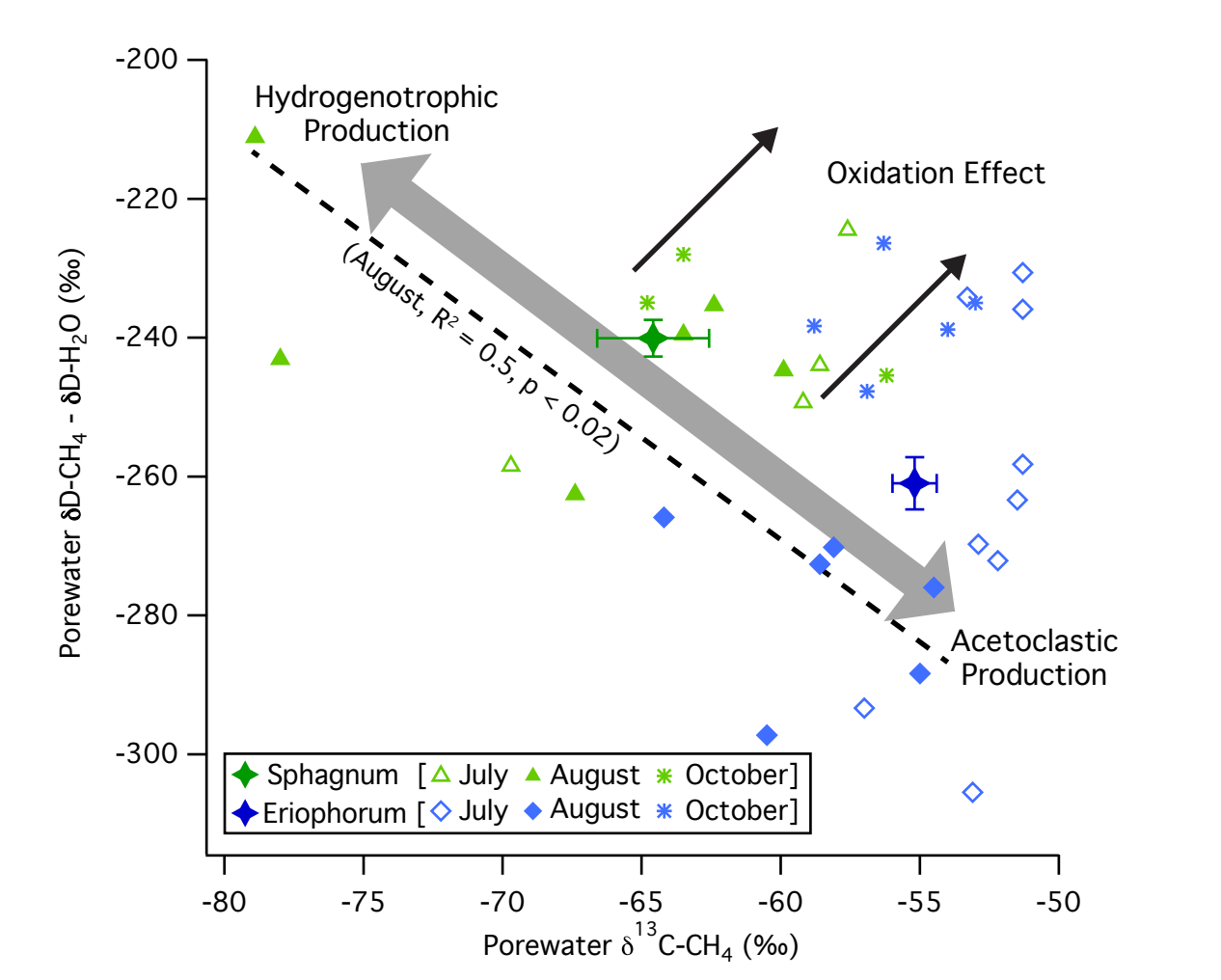
(Model 2), and  $\alpha_C$  from environmental variables (Model 3)

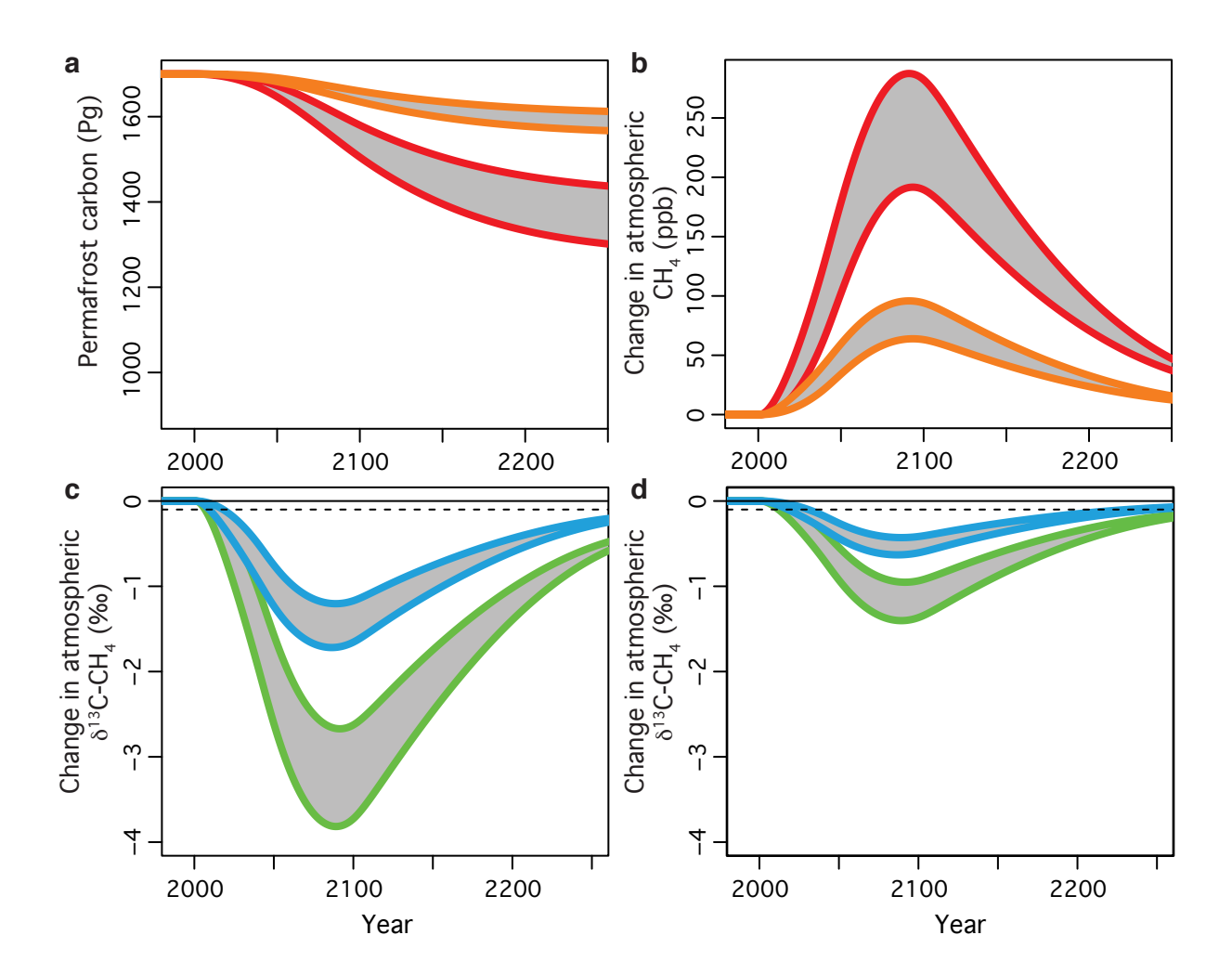
781











ED Table 1

Sample	Depth (cm)	рН	mM CO <sub>2</sub>	mM CH₄	$\delta^{13}CO_2$ ‰	δ <sup>13</sup> CH <sub>4</sub> ‰	$lpha_{ extsf{C}}$		
	July, 2011								
Sphagnum - M	13	4.1 (0.06)	3.02 (0.78)	0.09 (0.04)	-15.7 (1.6)	-62.2 (3.8)	1.050 (0.005)		
Sphagnum - D	19	4.2 (0.09)	3.50 (0.57)	0.15 (0.05)	-14.1 (0.6)	-62.2 (4.5)	1.051 (0.005)		
Eriophorum - S	3	5.8 (0.09)	2.29 (0.92)	0.18 (0.12)	-14.1 (1.1)	-52.1 (0.5)	1.040 (0.001)		
Eriophorum -M	7	5.6 (0.06)	3.06 (0.77)	0.28 (0.07)	-12.9 (1.0)	-52.6 (0.6)	1.042 (0.001)		
Eriophorum - D	24	5.6 (0.03)	3.56 (0.80)	0.36 (0.07)	-11.6 (1.7)	-53.3 (1.9)	1.044 (0.004)		
			Augus	t, 2011					
Sphagnum - M	21	4.2 (0.10)	4.89 (0.37)	0.23 (0.04)	-12.0 (1.5)	-66.7 (5.7)	1.059 (0.008)		
Sphagnum - D	26	4.1 (0.13)	4.80 (0.48)	0.23 (0.04)	-10.7 (1.6)	-69.9 (4.6)	1.064 (0.007)		
Eriophorum - S	3	5.7 (0.19)	1.62 (0.28)	0.06 (0.04)	-13.5 (0.5)	-60.0 (2.6)	1.049 (0.003)		
Eriophorum -M	7	5.7 (0.10)	1.93 (0.25)	0.10 (0.02)	-13.9 (0.4)	-56.6 (2.1)	1.045 (0.002)		
Eriophorum - D	26	5.6 (0.15)	3.58 (0.62)	0.31 (0.11)	-11.1 (2.4)	-55.9 (1.1)	1.047 (0.001)		
			Octobe	er, 2011					
Sphagnum - M	10	4.3 (0.06)	1.24 (0.42)	0.03 (0.02)	-16.4 (1.6)	-59.2 (6.5)	1.046 (0.006)		
Sphagnum - D	15	4.5 (0.10)	3.21 (0.90)	0.10 (0.04)	-13.8 (2.4)	-61.5 (2.7)	1.051 (0.0004)		
Eriophorum - S	3	5.9 (0.15)	2.15 (1.43)	0.19 (0.13)	-14.1 (1.0)	-56.4 (2.4)	1.045 (0.001)		
Eriophorum -M	7	5.9 (0.15)	2.71 (1.25)	0.29 (0.14)	-13.7 (1.6)	-57.8 (3.1)	1.047 (0.002)		
Eriophorum - D	26	5.7 (0.12)	3.84 (1.64)	0.53 (0.27)	-11.3 (3.1)	-58.1 (2.2)	1.050 (0.001)		

# ED Table 2

Sample	Candidatus <i>Methanoflorens</i> (otu-10747)	Methanobacterium (otu-3636)	Candidatus <i>Methanoregula</i> (otu-20819)	Methanosarcina (otu-7308)	Methanosaeta (otu-10220)	Methanosaeta (otu-15150)	
·	Hydrogenotrophic	Hydrogenotrophic	Hydrogenotrophic	Acetoclastic (facultative)	Acetoclastic (obligate)	Acetoclastic (obligate)	
			July, 2011				
Palsa – S	0.0	0.0	0.0	0.0	0.0	0.0	
Palsa – M	0.0	0.0	0.0	0.0	0.0	0.0	
Palsa – D	0.0	0.4	0.0	0.0	0.0	0.0	
Sphagnum – S	0.3	0.4	0.0	0.1	0.0	0.0	
Sphagnum – M	4.0	12.9	0.0	3.4	0.0	0.0	
Sphagnum – D	16.4	5.8	0.0	3.3	0.0	0.0	
Eriophorum – S	1.0	2.7	5.8	0.7	4.5	1.8	
Eriophorum – M	5.3	3.7	4.0	2.2	5.0	2.7	
<i>Eriophorum</i> – D	8.3	1.6	1.9	0.6	4.2	1.2	
			August, 2011				
Palsa – S	0.0	0.0	0.0	0.0	0.0	0.0	
Palsa – M	0.0	0.0	0.0	0.0	0.0	0.0	
Palsa – D	0.0	0.0	0.0	0.0	0.0	0.0	
Sphagnum – S	0.1	0.4	0.0	0.2	0.0	0.0	
Sphagnum – M	11.6	4.0	0.0	1.9	0.0	0.0	
Sphagnum – D	32.1	3.1	0.0	1.4	0.0	0.0	
Eriophorum – S	0.6	2.1	3.6	0.4	3.3	1.0	
Eriophorum – M	6.3	6.1	5.1	2.6	9.0	3.9	
<i>Eriophorum</i> – D	6.5	0.3	3.4	1.2	1.7	0.6	
			October, 2011				
Palsa – S	0.0	0.0	0.0	0.0	0.0	0.0	
Palsa – M	0.1	1.1	0.0	0.1	0.0	0.0	
Palsa – D	0.1	0.7	0.0	0.0	0.0	0.0	
Sphagnum – S	0.0	0.1	0.0	0.0	0.0	0.0	
Sphagnum – M	0.0	3.4	0.0	1.1	0.0	0.0	
Sphagnum – D	0.6	8.4	0.0	1.2	0.0	0.0	
Eriophorum – S	2.5	1.7	1.7	0.6	1.4	0.6	
Eriophorum – M	2.1	1.9	1.0	0.8	2.5	2.2	
<i>Eriophorum</i> – D	6.0	1.1	3.7	0.1	5.1	5.8	

ED Table 3

Site	Hydrogenotrophic	Acetoclastic (facultative)	Acetoclastic (obligate)	Other Archaea
	July	, 2011		
Palsa	35.9	2.9	0.0	61.2
Sphagnum (aerobic)*	83.1	15.5	0.0	1.4
Sphagnum (anaerobic) <sup>†</sup>	82.1	14.2	0.0	3.8
Eriophorum	39.5	4.2	21.4	34.9
	Augus	st, 2011		
Palsa	0.0	8.7	0.0	91.3
Sphagnum (aerobic)*	68.2	30.7	0.0	1.1
Sphagnum (anaerobic) <sup>†</sup>	91.2	6.1	0.0	2.8
Eriophorum	39.5	5.1	21.9	33.5
	Octob	er, 2011		
Palsa	56.5	2.6	0.4	40.5
Sphagnum (aerobic)*	65.7	24.0	0.7	9.6
Sphagnum (anaerobic) <sup>†</sup>	15.6	2.8	2.6	79.0
Eriophorum	35.8	2.4	27.6	34.2

ED Table 4

Variable	$R^2$	F-statistic	p-value
'M. stordalenmirensis'	0.58	54.09	<0.001
otu-3636*	0.00	0.01	0.926
otu-10220*	0.12	5.36	0.026
otu-20819 *	0.15	6.82	0.013
otu-15150 *	0.06	2.27	0.140
otu-7308 *	0.01	0.32	0.576
Hydrogenotrophic	0.44	30.63	<0.001
Acetoclastic (obligate)	0.12	5.23	0.028
Water table depth	0.44	31.1	<0.001
рН	0.19	8.97	0.005
Porewater CH <sub>4</sub> (mM)	0.00	0.07	0.796
Porewater DIC (mM)	0.25	13.33	0.001
Peat C:N	0.00	0.17	0.682
Peat %C	0.02	0.75	0.393
Peat %N	0.00	0.14	0.709
Peat $\delta^{13}$ C	0.13	5.99	0.019

ED Table 5

Variable	Coefficient	Std Error	t value	p value	Cumulative AIC
	Model 1 - ste	epwise regression	n, direction = l	both	
	$(R^2 = 0.81, F$	= 23.71 on 6 ar	nd 34 df, p <0.0	001)	
Water table depth	-0.0004	0.0001	-5.398	<0.001	-422.33
'M. stordalenmirensis'	0.0271	0.0084	3.221	0.002	-436.79
C:N	-0.0002	0.0001	-2.872	0.007	-438.80
Peat $\delta^{13}$ C	0.0014	0.0006	2.516	0.017	-440.71
DIC (mM)	0.0007	0.0005	1.396	0.171	-445.42
otu-3636*	-0.0271	0.0161	-1.345	0.188	-445.58
Intercept	1.089	0.0167	65.193	<0.001	-445.71
	Model 2 – signif	icant predictor v	ariables from r	model 1	
	$(R^2 = 0.79, F$	= 33.71 on 4 aı	nd 36 df, p <0.	001)	
Water table depth	-0.0004	0.0001	-5.202	<0.001	-425.11
'M. stordalenmirensis'	0.0351	0.0072	4.867	<0.001	-427.36
C:N	-0.0002	0.0001	-2.613	0.013	-440.97
Peat $\delta^{13}$ C	0.0014	0.0006	2.470	0.018	-441.67
Intercept	1.089	0.0164	66.583	<0.001	-446.09

# ED Table 6

Habitat	Area (ha)*	Annual Flux (g CH <sub>4</sub> m <sup>-2</sup> ) <sup>†</sup>	Annual Emission (kg CH <sub>4</sub> ) * <sup>,†</sup>	Estimated Emission from Hydrogenotrophy (kg CH <sub>4</sub> yr <sup>-1</sup> ) <sup>‡</sup>
Sphagnum	6.2	6.2	288.3	247.9 <sup>§</sup> - 282.5 <sup>  </sup>
Eriophorum	2.0	36.0	540.6	172.8 <sup>¶</sup> – 335.2 <sup>#</sup>
Total			828.9	420.7(51%) – 617.7 (75%)

ED Table 7

Sample name	Run #	Multiplex identifier (MID)
20110712_E_3_M	6	CGAGC
20110712_S_1_M	6	CGCAT
20110712_S_3_M	6	CGTAC
20110712_P_1_S	6	CGTGT
20110712_P_2_S	6	CTAGT
20110712_P_3_S	6	CTGAC
20110816_S_2_S	6	TACGC
20110816_S_1_D	6	TATGT
20110816_P_1_M	6	TCAGT
20111016_P_1_S	6	TCGAT

ED Table 8

Variable	Coefficient	Std Error	t value	p value	Cumulative AIC
Model 1	- stepwise regress	•			both
	$(R^2 = 0.75,$	F = 21.25 on 5	and 35 df, p <0.	001)	
Water table depth	0.299	0.07	4.512	<0.001	130.95
'M. stordalenmirensis'	-23.25	6.79	-3.426	0.002	124.01
Peat $\delta^{13}$ C	-1.51	0.54	-2.779	0.009	120.33
CH <sub>4</sub> (mM)	10.60	4.12	2.576	0.014	119.28
C:N	0.12	0.05	2.149	0.039	117.24
Intercept	-102.14	15.23	-6.705	<0.001	114.16
Model 2 - step	owise regression, d	ependent variab	le = 'M stordale	nmirensis', direct	tion = both
	$(R^2 = 0.53)$	s, F = 7.77 on 5 a	and 35 df, p <0.0	001)	
Water table depth	-0.0053	0.0015	-3.634	<0.001	-188.03
C:N	-0.0035	0.0010	-3.495	0.001	-188.88
DIC (mM)	0.0214	0.0106	2.025	0.050	-196.61
% C	0.0033	0.0018	1.799	0.081	-197.53
Soil temperature	0.0059	0.0040	1.483	0.147	-198.66
Intercept	-0.0558	0.0805	-0.692	0.493	-199.15
Mod	el 3 - stepwise regr	ession, depende	ent variable = $\alpha_{c}$	, direction = bot	h
	$(R^2 = 0.71,$	F = 21.71 on 4	and 36 df, p <0.	001)	
Water table depth	-0.0005	0.0001	-6.465	<0.001	-402.97
C:N	-0.0003	0.0001	-4.514	<0.001	-416.18
DIC (mM)	0.0015	0.0006	2.629	0.013	-427.36
Peat $\delta^{13}$ C	0.0017	0.0007	2.574	0.014	-427.63
Intercept	1.0990	0.0192	57.396	<0.001	-432.56